THE JOURNAL OF PHYSICAL CHEMISTRY B

Article

pubs.acs.org/JPCB

Influence of Replacing Si by Ge in the Chalcogenide Quaternary Sulfides $Ag_2In_2Si(Ge)S_6$ on the Chemical Bonding, Linear and Nonlinear Optical Susceptibilities, and Hyperpolarizability

A. H. Reshak,*[,†,‡] I. V. Kityk,[§,⊥] O. V. Parasyuk,[⊥] H. Kamarudin,[‡] and S. Auluck[∥]

[†]Institute of Complex Systems, FFPW, CENAKVA, University of South Bohemia in CB, Nove Hrady 37333, Czech Republic

[‡]School of Material Engineering, Malaysia University of Perlis, P.O. Box 77, d/a Pejabat Pos Besar, 01007 Kangar, Perlis, Malaysia

[§]Electrical Engineering Department, Czestochowa University of Technology, Armii Krajowej 17, Czestochowa, Poland

[∥]National Physical Laboratory, Dr. K. S. Krishnan Marg, New Delhi 110012, India

[⊥]Department of Inorganic and Physical Chemistry, Eastern European National University, 13 Voli Ave., Lutsk 43025, Ukraine

ABSTRACT: The linear and nonlinear optical properties of $Ag_2In_2SiS_6$ and $Ag_2In_2GeS_6$ are calculated so as to obtain further insight into the electronic properties. The influence of using different exchange correlation potentials and the effect of replacing Si by Ge on the geometry, chemical bonding, and on the optical properties are presented. There is notable increasing in the energy band gap when moving from LDA to GGA, EVGGA then to mBJ. The effect of replacing Si by Ge atom causes a geometric change, which leads to large changes in the linear as well as the nonlinear optical susceptibilities. For the linear optical properties, it causes to increase the amplitude of the left-hand hump of $\varepsilon_2^{average}(\omega)$ as well as a small shift of the main peak to lower energies. We have evaluated $\varepsilon_1^{average}(0)$ and find that a smaller energy gap yields a larger $\varepsilon_1(0)$ value. From the calculated refractive indices we obtained the birefringence, which is important for second harmonic generation (SHG) and optical parametric oscillation (OPO) as it is defined by the phase-matching condition. The second-order nonlinear optical susceptibilities, namely, the SHG are investigated for $\chi^{(2)}_{111}(\omega)$, $\chi^{(2)}_{122}(\omega)$, $\chi^{(2)}_{133}(\omega)$, $\chi^{(2)}_{221}(\omega)$, and $\chi^{(2)}_{331}(\omega)$. We find that $\chi^{(2)}_{111}(\omega)$ is the dominant component. The microscopic second order hyperpolarizability, β_{111}, for the dominant component $\chi^{(2)}_{111}(\omega)$ was obtained. We should emphasize that replacing Si by Ge enhances the linear and nonlinear optical susceptibilities so that $Ag_2In_2GeS_6$ shows higher values of the linear and nonlinear optical susceptibilities and β_{111} in comparison to $Ag_2In_2SiS_6$.

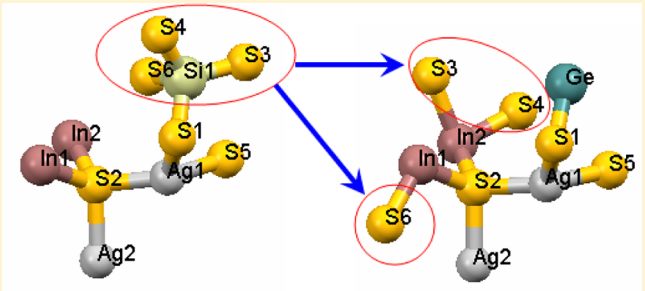

1. INTRODUCTION

The chalcogenides form a large group of semiconducting materials with diverse properties. They have received much attention due to their possible applications.[1−12] The most interesting feature of the chalcogenide compounds is the energy gap arises from the p-chalcogenic delocalized states of the valence band and the relatively more localized s- and d-cationic states of the conduction band.[13] The chalcogenides possess non-centrosymmetric crystal structures, which makes them promising nonlinear optical materials.[14] Recently, complex spectral studies of the near-band gap and photoconductive spectra for novel $Ag_2In_2Ge(Si)S_6$ single crystals were presented.[15] The spectral dependences of photoconductivity illustrate the existence of spectral maxima within 450−540 nm and 780−920 nm. $Ag_2In_2GeS_6$ possess different geometry than $Ag_2In_2SiS_6$.[15,16] This geometric variation leads to large changes in the linear as well as the nonlinear optical properties.[17]

Yet up to now, there is no comprehensive work that investigates the linear and nonlinear optical susceptibilities of the $Ag_2In_2Ge(Si)S_6$ single crystals. Moreover, we would like to see the effect of different exchange correlation potentials on the calculated optical properties. It would be interesting to see the effect of replacing Si by Ge on the electronic properties and dispersion of second order optical susceptibilities. Ab initio calculations have been successfully used to obtain different electronic properties of materials. The structural parameters and dynamical properties of crystals determine a wide range of microscopic and macroscopic behavior: diffraction, sound velocity, elastic constants, Raman and infrared absorption, inelastic neutron scattering, specific heat, etc. Therefore, we thought it worthwhile to perform ab initio calculations using a full potential method to investigate the influence of replacing Si by Ge on the chemical bonding and hence on the linear and nonlinear optical susceptibilities of these single crystals.

2. SINGLE CRYSTAL PREPARATION

The single crystals preparation is described in detail in our previous work.[16] Now let us recall the main features of the

Received: December 2, 2012
Revised: January 29, 2013

   dx.doi.org/10.1021/jp311842v | J. Phys. Chem. B XXXX, XXX, XXX−XXX

single crystals preparation; the single crystal growth of the incongruently melting compounds is most favorably realized by the solution−melt method. The selection of the solvent is very important in the application of this method. In this work, we have grown the crystals of the quaternary compounds using the excess of Ag_2S and $Si(Ge)S_2$ (vs stoichiometry) as the solvent. The starting composition was selected from the field of the primary crystallization of the compounds that form in the quasi-ternary systems $Ag_2S-In_2S_3-Si(Ge)S_2$.[14] The 15 g batches of the selected composition were prepared from high-purity elements (at least 99.999 wt %). At the first stage, the preliminary synthesis of the alloys was performed using the technique described in ref 14. After cooling the ampule to room temperature, obtained compact alloy was crushed into powder in an agate mortar and then poured into a quartz container with a conical bottom. Taking into account the volatile components of the composition, the volume of the growth container was decreased as much as possible using silica plug seal with a diameter close to the inner diameter of the container. After evacuation, the seal was soldered to the inner walls of the container. Thus, a prepared container was placed in a two-zone growth furnace. The crystal growth was performed by slowly lowering (7 mm/day) the container into the furnace with a stable temperature profile. The furnace gradient at the solid−melt interface was ∼1.8 K/cm. After complete crystallization of the melt, both zones of the furnace were synchronously cooled at the rate of 100 K/day to room temperature. Obtained boules consisted of two parts. The lower (conical) part contained accretions of single-crystalline blocks of the linear dimensions of several millimeters, and the upper part was the crystallized eutectic.

The obtained bulk crystals were analyzed by X-ray powder diffraction, which proved the formation of the well-defined $Ag_2In_2SiS_6$ and $Ag_2In_2GeS_6$ compounds. The reflections of the powder (prepared by crushing the pure $Ag_2In_2SiS_6$ and $Ag_2In_2GeS_6$ crystals) X-ray pattern, acquired in the Bragg−Brentano geometry using the CuK_α radiation (DRON 4-13 diffractometer), could be indexed in the *Cc* space group. Experimental and calculated diffraction patterns of $Ag_2In_2SiS_6$ and LT-$Ag_2In_2GeS_6$, as well as their difference, are presented in our previous work.[16] The lattice periods agree well with those reported in ref 14.

3. COMPUTATIONAL DETAILS

Recently we have synthesized $Ag_2In_2GeS_6$ compound and investigated the electronic structure.[15,16] Later, we replace Ge by Si atom and synthesized a new compound, namely, $Ag_2In_2SiS_6$ and study the effect of replacing Ge by Si atom on the electronic structure.[16] In the current work, we are interested to study the influence of replacing Si by Ge on the linear and nonlinear optical susceptibilities from the point of view of the geometrical and chemical bonding changes since the optical dielectric function helps to obtain further insight into the electronic structure. These optical susceptibilities were calculated from the relaxed structure of $Ag_2In_2SiS_6$ and $Ag_2In_2GeS_6$ compounds. To solve the Kohn−Sham DFT equations, the all-electron full potential linearized augmented plane wave (FP-LAPW) method within the framework of the WIEN2K code[18] was used. In order to achieve the self-consistency, the values of nonoverlapping spheres of muffin-tin radius (R_{mt}) are chosen to be 2.50 a.u. for Ag, 2.34 a.u. for In, and 1.99 a.u. for Si and S. These values were chosen in such a way that the spheres did not overlap. The convergence of the self-consistent calculations is taken with respect to the total charge of the system with a tolerance of 0.0001 electrons. In order to get the total energy convergence, the basis functions in the interstitial region were expanded up to $R_{mt} \times K_{max} = 7.0$ and inside the atomic spheres for the wave function. The maximum value of l were taken as $l_{max} = 10$, while the charge density is Fourier expanded up to $G_{max} = 20$ (a.u.)$^{-1}$. We have used 35 **k**-points in the irreducible Brillouin zone for structural optimization. For calculating the linear optical susceptibilities, a denser mesh of 800 **k**-points was used, and 1500 **k**-points for nonlinear optical susceptibilities was used.

4. ENERGY BAND GAP

Using spectrophotometer Ocean optics with spectra resolution up to 1 nm, we have measured the energy gaps, and we have found that they are equal to 1.96 eV for $Ag_2In_2GeS_6$ and 2.0 eV for $Ag_2In_2SiS_6$. It is crucial that these gaps are substantially disordered by the existence of a huge number of defect states.

For calculating the energy gap, four kinds of exchange correlation (XC) potentials were used. First, we have employed the local density approximation (LDA) by Ceperley−Alder (CA),[19] which gives a very small energy gap of about 0.76 (0.67) eV for $Ag_2In_2SiS_6$ ($Ag_2In_2GeS_6$) in comparison with our measured gap 2.0 (1.96) eV. In order to overcome this underestimation, we used the generalized gradient approximation (GGA).[20] GGA enhanced the value of the energy gap 0.98 (0.85) eV, but it is still far from the measured ones. We found that the Engel−Vosko generalized gradient approximation (EV-GGA)[21] significantly enhanced the value of the energy gap to be 1.57 (1.53) eV, and the modified Becke−Johnson potential (mBJ)[22] is successful in bringing the energy gap 1.98 (1.88) eV very close to the measured gap 2.0 (1.96) eV.

5. RESULTS AND DISCUSSION

5.1. Chemical Bonding Properties. Looking at Figure 1a, in $Ag_2In_2SiS_6$ single crystal the atoms, S3, S4, and S6 are attached to Si atom with bond lengths 2.122 (Si−S3), 2.131 (Si−S4), and 2.136 Å (Si−S6) and bond angles 109.11° (S3−Si−S4), 106.68° (S6−Si−S4), and 109.78° (S6−Si−S3). When we replace Si by Ge, both of S3 and S4 atoms immigrate to join In2 atom with the bond lengths 2.513 (In2−S3) and 2.487 Å (In2−S4) and bond angle 91.62° (S4−In2−S3), whereas S6 atom immigrates to join In1 atom with bond length 2.493 Å and angle 110.65° (S6−In1−S2). In $Ag_2In_2SiS_6$, both of In1 and In2 atoms are connected to S2 atom only with bond length 2.500 (In2−S2) and 2.490 Å (In1−S2) and bond angle 96.04° (In1−S2−In2) in comparison to the bond lengths and angle of the same atoms in $Ag_2In_2GeS_6$ single crystal 2.516 (In2−S2) and 2.502 Å (In1−S2) and 97.82° (In1−S2−In2); see Figure 1a. Both S3 and S4 form partially ionic and partially covalent bonds with In2, while S6 form strong ionic and weak covalent bonds with In1. When the bond length is increased, the overlapping of the orbitals become less, and according to Pauli exclusion principle, some of the band states are shifted to lower energy, which is one factor of decreasing the band gap. We should emphasize that the single crystal $Ag_2In_2SiS_6$ possesses an energy gap equal to about 2.0 eV, which is slightly bigger than that obtained for $Ag_2In_2GeS_6$ (1.96 eV) in comparison with the theoretical values (1.95 eV for $Ag_2In_2SiS_6$ and 1.88 eV for $Ag_2In_2GeS_6$) (see Figure 1b). The overall reduction/increase in gap correlates with an overall weakening/strength of the bonds and therefore with a smaller/greater bonding antibonding

dx.doi.org/10.1021/jp311842v | J. Phys. Chem. B XXXX, XXX, XXX−XXX

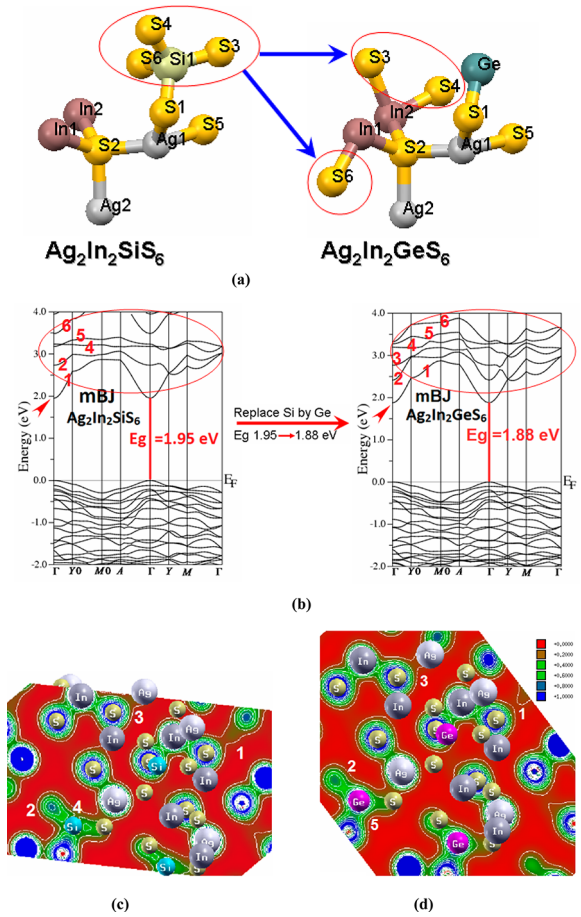

Figure 1. (a) Asymmetric unit of $Ag_2In_2SiS_6$ in comparison with $Ag_2In_2GeS_6$. (b) The calculated band structure of $Ag_2In_2SiS_6$ in comparison with $Ag_2In_2GeS_6$ using mBJ. The electron charge density distribution was calculated for the (101) crystallographic plane for (c) $Ag_2In_2GeS_6$ and (d) $Ag_2In_2SiS_6$ single crystals.

splitting. Alternatively, the differences in the energy gap could be caused by a different degree of Coulomb self-interaction. Also increasing the bond lengths decreases the optical gap. Thus, the change in the bond length strongly influences the optical properties.

During replacement of Si atom by Ge atom, all the bands in the conduction band are shifted slightly toward lower energies with respect to Fermi energy while the valence bands are almost unchanged (see Figure 1b); that could be another reason of reducing the energy band gap and hence enhancing the optical properties. The valence band is prevailingly originated from Ag-d states and S-p orbitals. The S-p states are mainly concentrated in the valence band with small amount in the conduction band. The conduction band comprises In-s and S-p states showing ionic bond character. Also, it is worth mentioning that Ag-d states are hybridized with S-p states forming preliminary ionic bonds. In-p hybridizes with Ag-s/p, while In-s hybridizes with Si-s/p states. Hence some electrons from Ag, In, Si, and S atoms are transferred into valence bands and contribute in covalence interactions. The interaction due to the strong hybridization and the covalent bond is defined by the degree of hybridization. Hence, there is a strong covalent bonding between the atoms that exhibit strong hybridization. To support this statement, we have taken a more careful look at the bonding situation since the existence of real hybridization between states of atoms should lead to covalent bond's origin between these atoms. Thus, we recall the electron charge density distribution of $Ag_2In_2Si(Ge)S_6$.[16] We have chosen the (101) crystallographic plane to depict principal charge transfer. It is clear that there exists partial ionic and strong covalent bonds and vice versa between Ag−S, In−S, Si−S, and Ge−S atoms depending on Pauling electronegativity difference of S (2.58), Ge (2.01), Ag (1.93), Si (1.9), and In (1.78) atoms. These contour plots show that the majority of Ag, In, Si, and Ge electronic charge is transferred to the S atom. One can see that the S atoms are more electronegative with respect to Ag, In, Si, and Ge atoms, and more charge accumulates near S atoms along the bonds, and the charge around S atoms are uniformly space distributed. This can be visually observed by the color charge density scale where blue color (+1.00) corresponds to the maximum charge accumulation site. The space electronic charge density contour plots around Ag, In, Ge, Si, and S atoms are spherical. It is crucial that Ag−S, Ge−S, Si−S, and In−S lines connecting these atoms show partial covalent and strong ionic features because the small electronegativity difference between Ag−S (0.65), Ge−S (0.57), Si−S (0.68), and In−S (0.8). Comparing Figure 1c,d, in the case of $Ag_2In_2GeS_6$, the S atom near the label # 1 shows an ionic bond with the nearest Ag atom, whereas in $Ag_2In_2SiS_6$, the S atom shows a covalent bond with the nearest Ag atom. Near the label #2, the bond between Ge and S atoms in $Ag_2In_2GeS_6$ is weak covalent, while S form a strong covalent bond with Si in $Ag_2In_2SiS_6$. The covalent bonding possess the maximum values of the charge density between the interacting atoms contrary to the ionic ones, which require effective charge transfer. We should emphasize that, by replacing an atom by another, the properties of valence shell charge carrier (VSCC) changes.[23] If the loss of this charge concentration and its associated excess of potential energy were not compensated, the energy of the atoms would increase significantly and, in addition, the zero-flux surface condition would no longer be fulfilled. Thus, the effect of replace Si by Ge leads to change the properties of VSCC for S atom (labeled #3) and Ge atom (labeled #5), i.e., the charge density round S and Ge increases in $Ag_2In_2GeS_6$ comparatively to $Ag_2In_2SiS_6$.

5.2. Linear Optical Susceptibilities. Since the optical dielectric function helps to obtain further insight into the electronic structure, we recall some figures from our previous work[16] as illustrated in Figure.1. These figures confirm the influence of replacing Si by Ge atom on the electronic band structure dispersion in **k**-space and hence on the optical transitions according to the dipolar selection rule, which allows only transitions corresponding to a change in the angular momentum quantum number l by unity. $Ag_2In_2GeS_6$ and $Ag_2In_2SiS_6$ crystallize in *Cc* monoclinic space group. This space groups allows several nonzero tensor components for the second-order dielectric tensor corresponding to the electric field $\vec{E}$ being directed along **a**, **b**, and **c**-crystallographic axes. We will assume that these are the *x,y,z* components. We will concentrate only on the principal diagonal tensor components, $\varepsilon^{xx}(\omega)$, $\varepsilon^{yy}(\omega)$, and $\varepsilon^{zz}(\omega)$, which completely define the dispersion of linear optical susceptibilities. To analyze the spectral structures of $\varepsilon_2^{xx}(\omega)$, $\varepsilon_2^{yy}(\omega)$, and$\varepsilon_2^{zz}(\omega)$ one needs to look at the magnitude of the optical matrix elements. The observed structures of $\varepsilon_2^{xx}(\omega)$, $\varepsilon_2^{yy}(\omega)$, and $\varepsilon_2^{zz}(\omega)$ correspond to those transitions that have large optical matrix elements. It is worthy to emphasize that there is a notable increase in the energy band gap on moving from LDA to GGA, EVGGA then

dx.doi.org/10.1021/jp311842v | J. Phys. Chem. B XXXX, XXX, XXX−XXX

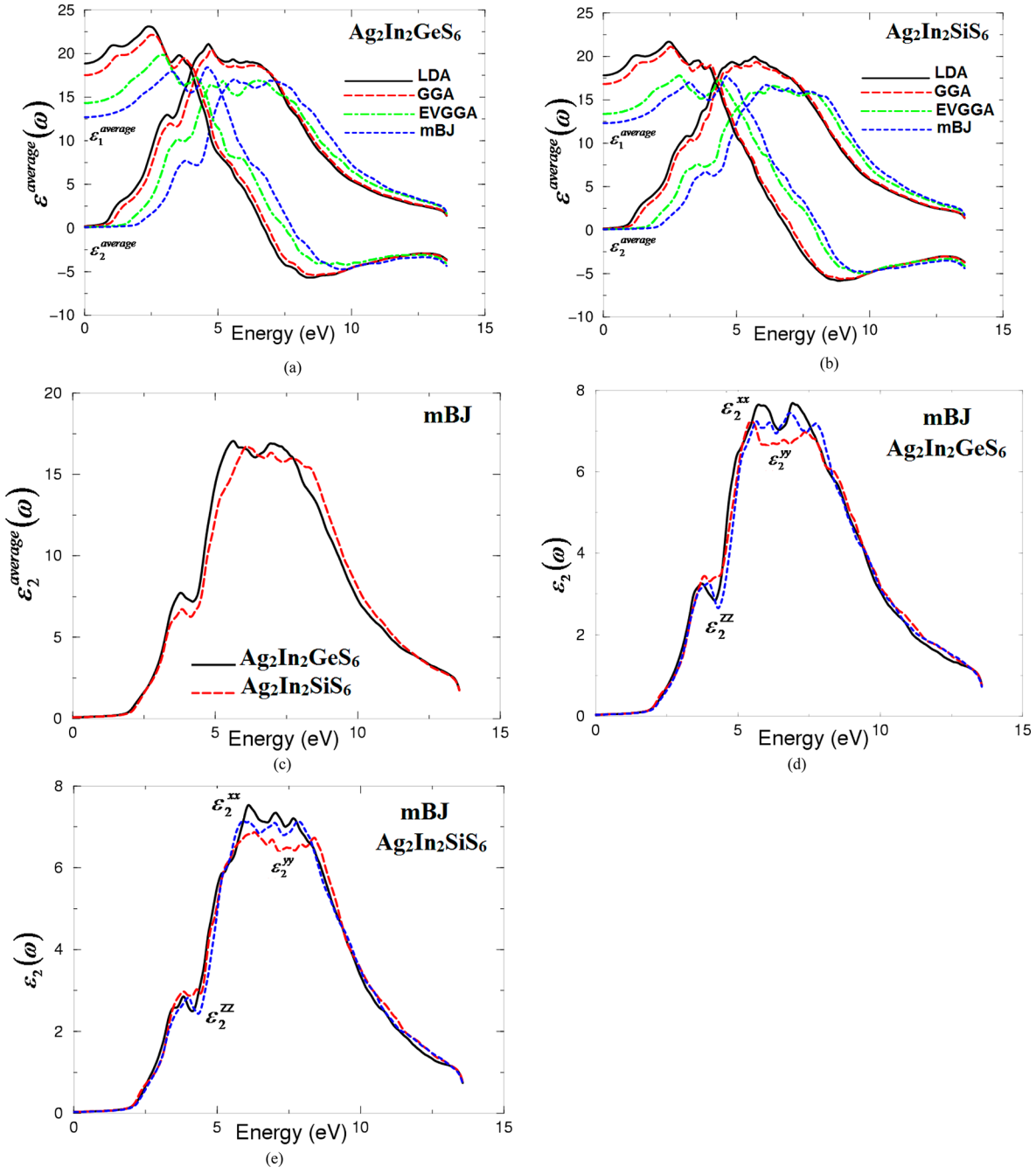

Figure 2. (a) Calculated $\varepsilon_2^{average}(\omega)$ using LDA, GGA, EVGGA, and mBJ for $Ag_2In_2GeS_6$. (b) Calculated $\varepsilon_2^{average}(\omega)$ using LDA, GGA, EVGGA, and mBJ for $Ag_2In_2SiS_6$. (c) Calculated $\varepsilon_2^{average}(\omega)$ using mBJ for $Ag_2In_2GeS_6$ in comarsion with $Ag_2In_2SiS_6$. (d) Calculated $\varepsilon_2^{xx}(\omega)$ (dark solid curve, black), $\varepsilon_2^{yy}(\omega)$ (light dashed curve, red), and $\varepsilon_2^{zz}(\omega)$ (light dotted dashed curve, blue) dispersion spectra using mBJ for $Ag_2In_2GeS_6$. (e) Calculated $\varepsilon_2^{xx}(\omega)$ (dark solid curve, black), $\varepsilon_2^{yy}(\omega)$ (light dashed curve, red), and $\varepsilon_2^{zz}(\omega)$ (light dotted dashed curve, blue) dispersion spectra using mBJ for $Ag_2In_2SiS_6$.

to mBJ and that the optical transitions occur according to the dipolar selection rule, which allows only transitions corresponding to a change in the angular momentum quantum number l by unity. In order to demonstrate the effect of these XC on optical dispersions, we have calculated $\varepsilon_2^{average}(\omega)$ using the expression given in ref 24. Figure 2a,b shows this effect on $\varepsilon_2^{average}(\omega)$ for the title compounds. It is clear that the $\varepsilon_2^{average}(\omega)$ dispersion is spectrally shifted to higher energies with reduced amplitude during successive moving from LDA to GGA, EVGGA then to mBJ. The optical absorption edges for each of LDA, GGA, EVGGA, and mBJ are situated at 0.67 (0.76), 0.85 (0.89), 1.53 (1.57), and 1.88 (1.98) eV in comparison with the experimental value 1.98 (2.0) eV for $Ag_2In_2GeS_6$ ($Ag_2In_2SiS_6$), respectively. These points define critical points or the minimal thresholds for optical transitions between VBM and CBM. The edges of optical absorption can be assigned to $\Gamma_v-\Gamma_c$ band energy splitting. Since these figures show that mBJ brings the theoretical value of the energy gap very close to the experiment, we will show our results obtained with mBJ.

Now let us demonstrate the effect of replacing Si by Ge atom on the optical dispersion; first, we illustrate $\varepsilon_2^{average}(\omega)$ of $Ag_2In_2SiS_6$ along with that obtained for $Ag_2In_2GeS_6$ in Figure

dx.doi.org/10.1021/jp311842v | J. Phys. Chem. B XXXX, XXX, XXX−XXX

Table 1. Calculated Energy Band Gap in Comparison with the Experimental Value, $\varepsilon_1^{xx}(0)$, $\varepsilon_1^{yy}(0)$, $\varepsilon_1^{zz}(0)$, $\varepsilon_1^{average}(0)$, $n^{xx}(0)$, $n^{yy}(0)$, $n^{zz}(0)$, $n^{average}(0)$, and $\Delta n(0)$, without and with Scissors Corrections

	(LDA) $Ag_2In_2GeSi_6$ ($Ag_2In_2SiSi_6$)	(GGA) $Ag_2In_2GeSi_6$ ($Ag_2In_2SiSi_6$)	(EVGGA) $Ag_2In_2GeSi_6$ ($Ag_2In_2SiSi_6$)	(mBJ) $Ag_2In_2GeSi_6$ ($Ag_2In_2SiSi_6$)	(exptl) $Ag_2In_2GeSi_6$ ($Ag_2In_2SiSi_6$)
E_g	0.67 (0.76) eV	0.85 (0.89) eV	1.53 (1.57) eV	1.88 (1.98) eV	1.96(2.0) eV
$\varepsilon_1^{xx}(0)$	8.19 (7.67)	7.61 (7.29)	6.33 (5.81)	5.53 (5.45)	
$\varepsilon_1^{yy}(0)$	8.07 (7.66)	7.48 (7.19)	6.02 (5.71)	5.41 (5.25)	
$\varepsilon_1^{zz}(0)$	7.87 (7.45)	7.31 (7.02)	5.95 (5.61)	5.35 (5.19)	
$\varepsilon_1^{average}(0)$	18.9 (17.8)	17.5 (16.8)	14.3 (13.4)	12.7 (12.3)	
$n^{xx}(0)$	2.86 (2.77)	2.76 (2.70)	2.57 (2.41)	2.35 (2.31)	
$n^{yy}(0)$	2.84 (2.76)	2.74 (2.68)	2.45 (2.39)	2.33 (2.29)	
$n^{zz}(0)$	2.81 (2.73)	2.71 (2.65)	2.44 (2.37)	2.31 (2.28)	
$n^{average}(0)$	6.86 (6.45)	6.39 (6.26)	5.79 (5.59)	5.45 (5.36)	
$\Delta n(0)$	0.04 (0.035)	0.04 (0.04)	0.07 (0.03)	0.03 (0.02)	

2c. It is clear that the spectral features of $\varepsilon_2^{average}(\omega)$ for both crystals are similar except a small increase in the amplitude of the left-hand hump of $\varepsilon_2^{average}(\omega)$ $Ag_2In_2GeS_6$ as well as a small spectral shift of the main peak toward lower energies. This difference could be attributed to the fact that replacing Si by Ge leads to immigrate the S3, S4, and S6 atom,s which are directly connected to Si atom in $Ag_2In_2SiS_6$ to join In1 and In2 atoms in $Ag_2In_2GeS_6$ leaving the ends of In1 and In2 atoms in $Ag_2In_2GeS_6$ opened (see Figure 1a). Thus, following Figure 1b, there is clear differences in the band splitting of the CB of $Ag_2In_2SiS_6$ with respect to $Ag_2In_2GeS_6$, and hence the optical transitions are differed accordingly.

The principal complex tensor components $\varepsilon_2^{xx}(\omega)$, $\varepsilon_2^{yy}(\omega)$, and $\varepsilon_2^{zz}(\omega)$ are plotted in Figure 2d,e. These principal complex tensor components for the investigated compounds show considerable anisotropy with respect to the left-hand hump and the main peak. That is the main reason for the increase in the birefringence determining the efficiency of the phase matching conditions, which are necessary for observation of the second harmonic generation (SHG).

Knowing the imaginary part dispersion for the principal complex tensor components helps to obtain the real part of the corresponding principal complex tensor components by means of Kramers–Kronig transformation.[25] To demonstrate the effect of using different XC on the real part of the tensor components, $\varepsilon_1^{average}(\omega)$ of $Ag_2In_2GeS_6$ and $Ag_2In_2SiS_6$ are plotted in Figure 2a,b. Following these figures, one can conclude that there is significant effect with moving from LDA to GGA, EVGGA to mBJ. The whole spectral structure of $\varepsilon_1^{average}(\omega)$ dispersion is spectrally shifted toward higher energies with reduced amplitude in agreement with our observation regarding $\varepsilon_2^{average}(\omega)$ (Figure 2a,b). As a remarkable finding, the static dielectric constant $\varepsilon_1^{average}(0)$ decreases on moving from LDA to GGA, EVGGA to mBJ. We should emphasis that a smaller energy gap yields a larger $\varepsilon_1(0)$ value. This could be explained on the basis of the Penn model.[26] Penn proposed a relationship between $\varepsilon(0)$ and E_g, $\varepsilon(0) \approx 1 + (\hbar\omega_p/E_g)^2$. E_g is some kind of averaged energy gap that could be related to the real energy gap. It is clear that $\varepsilon(0)$ is inversely proportional with E_g. Hence a smaller E_g yields a larger $\varepsilon(0)$. The values of $\varepsilon_1^{average-LDA}(0)$, $\varepsilon_1^{average-GGA}(0)$, $\varepsilon_1^{average-EVGGA}(0)$, and $\varepsilon_1^{average-mBJ}(0)$ are listed in Table 1. Figure 3a,b shows the real parts of the principal complex tensor components $\varepsilon_1^{xx}(\omega)$, $\varepsilon_1^{yy}(\omega)$, and $\varepsilon_1^{zz}(\omega)$. One can see that there is a considerable anisotropy in the energy regions from 4.0 to 6.0 eV and 7.0 to 8.5 eV.

We have also obtained the birefringence (the difference between the extraordinary and ordinary refraction indices) from the linear response functions from which the anisotropy of the refractive indices is defined. To obtain the values of the birefringence, first we need to evaluate the refractive indices. Thus, we have calculated $n^{xx}(\omega)$, $n^{yy}(\omega)$, and $n^{zz}(\omega)$ dispersions as illustrated in Figure 3c,d. To demonstrate the influence of replacing Si by Ge atom on the refractive indices, we have evaluate $n^{average}(\omega)$ for the investigated crystals. One can see that replacing Si by Ge atom increase the birefringence's value as demonstrated in Figure 3e and Table 1. The value of the birefringence and the corresponding refractive indices at the static limit are presented in Table 1. To the best of our knowledge, there is no experimental data for the birefringence, and the refractive indices are available in the literatures to verify our calculations. However, we have done similar calculations on many compounds,[27−32] and we have found good agreement with experiment. Thus, our calculated refractive indices and the birefringence obtained using mBJ are expected to be much closer to the experimental values.

5.3. Nonlinear Optical Susceptibilities. Let us turn our concern to investigate the second-order nonlinear optical (NLO) susceptibilities dispersion, namely, the optical second harmonic generation (SHG). We will explore the influence of using different XC on the NLO susceptibilities, as well as the influence of replacing Ge by Si atom. The nonlinear optical susceptibility is very sensitive to small changes in the band gap and band structure than the linear optical susceptibility. Since mBJ XC potential gives the energy gap in excellent agreement with experiment. Thus, we will show only the results of SHG obtained with mBJ. When the calculated energy gap is not close to the experiment, we can introduce a quasi-particle self-energy correction at the level of scissors operators in which the energy bands are rigidly shifted to merely bringing the calculated energy gap closer to the experimental value.[33] The investigated compounds show a monoclinic space group. This space groups allows only five nonzero complex second-order nonlinear optical susceptibility tensor components. These are $\chi_{111}^{(2)}(\omega)$, $\chi_{222}^{(2)}(\omega)$, $\chi_{133}^{(2)}(\omega)$, $\chi_{221}^{(2)}(\omega)$, and $\chi_{331}^{(2)}(\omega)$. Figure 4a,b depicts the dispersion of these components, following these figures, one can say that $\chi_{111}^{(2)}(\omega)$ is the dominant component since it brings the highest value of $|\chi_{ijk}^{(2)}(\omega)|$ among the other components (see Table 2). Table 2 shows the calculated $|\chi_{ijk}^{(2)}(0)|$ and $|\chi_{ijk}^{(2)}(\omega)|$ in pm/V at λ = 1064 nm along with d_{ijk} values. The calculated values in this table were evaluated using mBJ. Now let us demonstrate the effect of replacing Si by Ge atom on the SHG of the dominant component; Figure 4c,d shows that the

dx.doi.org/10.1021/jp311842v | J. Phys. Chem. B XXXX, XXX, XXX−XXX

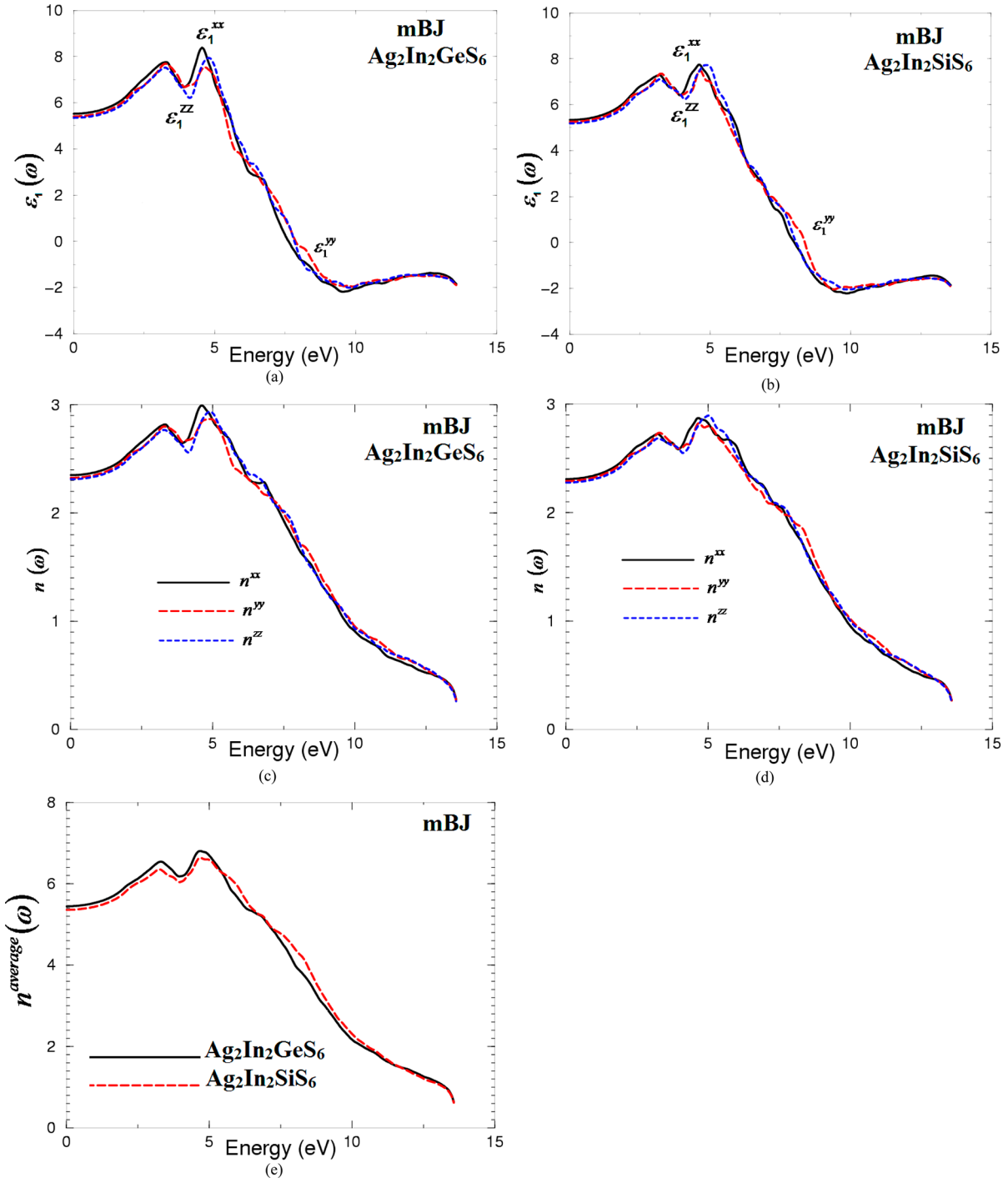

Figure 3. (a) Calculated $\varepsilon_2^{xx}(\omega)$ (dark solid curve, black), $\varepsilon_2^{yy}(\omega)$ (light dashed curve, red), and $\varepsilon_2^{zz}(\omega)$ (light dotted dashed curve, blue) dispersion spectra using mBJ for $Ag_2In_2GeS_6$. (b) Calculated $\varepsilon_2^{xx}(\omega)$ (dark solid curve, black), $\varepsilon_1^{yy}(\omega)$ (light dashed curve, red), and $\varepsilon_1^{zz}(\omega)$ (light dotted dashed curve, blue) dispersion spectra using mBJ for $Ag_2In_2SiS_6$. (c) Calculated $n^{xx}(\omega)$ (dark solid curve, black), $n^{yy}(\omega)$ (light dashed curve, red), and $n^{zz}(\omega)$ (light dotted dashed curve, blue) dispersion spectra using mBJ for $Ag_2In_2GeS_6$. (d) Calculated $n^{xx}(\omega)$ (dark solid curve, black), $n^{yy}(\omega)$ (light dashed curve, red), and $n^{zz}(\omega)$ (light dotted dashed curve, blue) dispersion spectra using mBJ for $Ag_2In_2SiS_6$. (e) Calculated $n^{average}(\omega)$ using mBJ for $Ag_2In_2GeS_6$ in comarsion with $Ag_2In_2SiS_6$;.

dispersion of the spectral structure of the $\mathrm{Im}\chi_{111}^{(2)}(\omega)$ and $|\chi_{111}^{(2)}(\omega)|$ for $Ag_2In_2GeS_6$ and $Ag_2In_2SiS_6$ are different. This difference could be attributed to the fact that replacing Si by Ge leads to immigrate the S3, S4, and S6 atoms, which directly connect to Si atom in $Ag_2In_2SiS_6$ to join In1 and In2 atoms in $Ag_2In_2GeS_6$ leaving the ends of In1 and In2 atoms in $Ag_2In_2GeS_6$ open (see Figure 1a).

To make a comparison between the calculated and experimental values of the SHG, we have performed some experimental studies of SHG. Because the samples were of small sizes, we have used powder technique to determine the effective second order susceptibilities. The measurements of the SHG were performed using the powder Kurtz Perry method.[34] Samples with sizes within 100−300 μm were put between the

dx.doi.org/10.1021/jp311842v | J. Phys. Chem. B XXXX, XXX, XXX−XXX

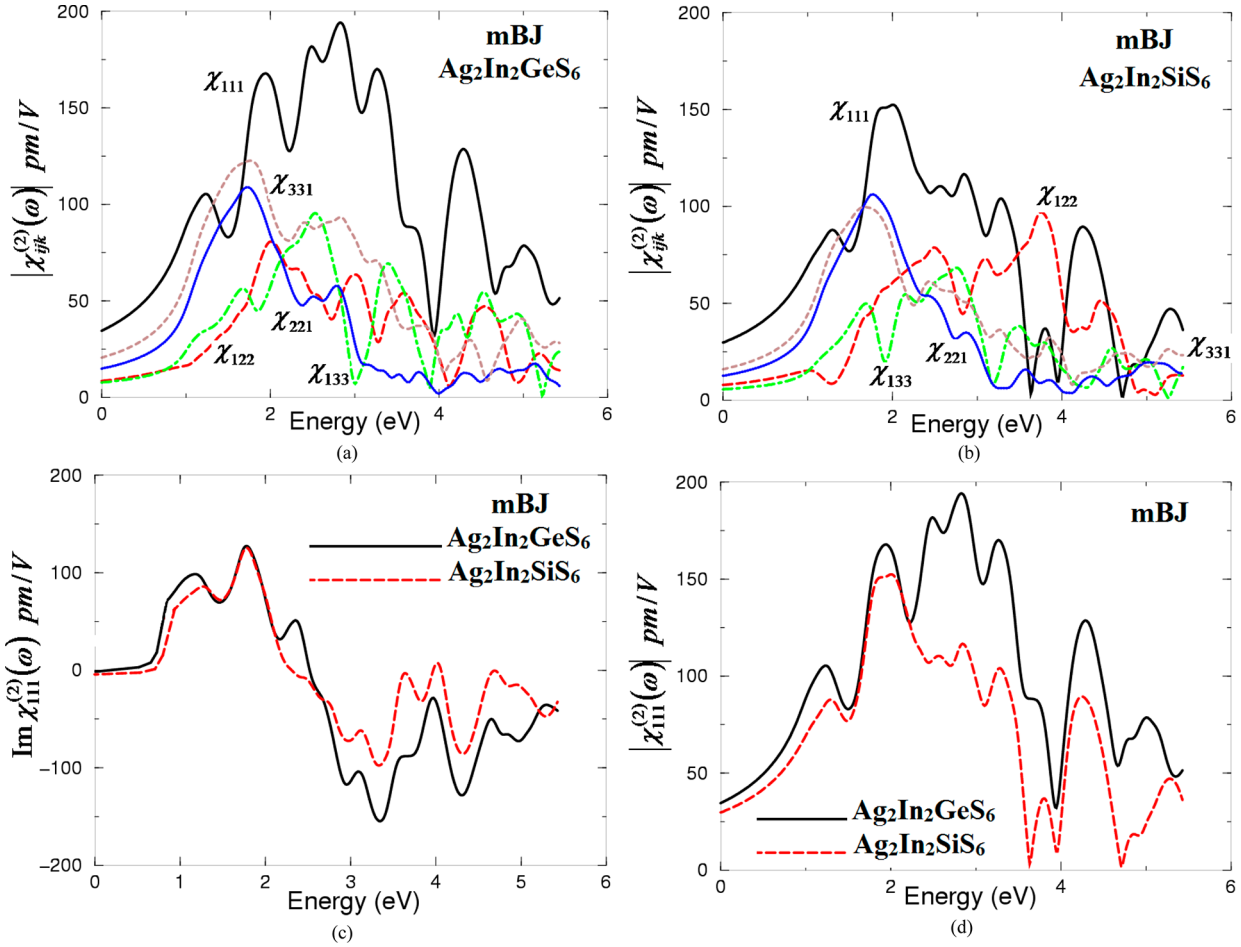

Figure 4. (a) Calculated $|\chi^{(2)}_{ijk}(\omega)|$ for the five components of $Ag_2In_2GeS_6$ using mBJ. (b) Calculated $|\chi^{(2)}_{ijk}(\omega)|$ for the five components of $Ag_2In_2SiS_6$ using mBJ. (c) $\mathrm{Im}|\chi^{(2)}_{111}(\omega)|$ for $Ag_2In_2GeS_6$ in comarsion with $Ag_2In_2SiS_6$. (d) $|\chi^{(2)}_{111}(\omega)|$ for $Ag_2In_2GeS_6$ in comarsion with $Ag_2In_2SiS_6$.

Table 2. Calculated $|\chi^{(2)}_{ijk}(\omega)|$ and $|\chi^{(2)}_{ijk}(\omega)|$ in pm/V at λ = 1064 nm along with d_{ijk} Values Where 1 pm/V = 2.387 × 10^{-9} esu; the Calculated Values in This Table Are Done Using mBJ

tensor components	theory $\chi^{(2)}_{ijk}(0)$ in pm/V	theory d_{ijk} = 0.5 $\chi^{(2)}_{ijk}(0)$ in pm/V	theory $\chi^{(2)}_{ijk}(\omega)$ in pm/V at λ = 1064 nm	theory d_{ijk} = 0.5 $\chi^{(2)}_{ijk}(\omega)$ in pm/V at λ = 1064 nm
$\|\chi^{(2)}_{111}(\omega)\|$ $Ag_2In_2GeSi_6$ ($Ag_2In_2SiSi_6$)	35.0 (30.0)	17.5 (15.0)	105.0 (81.0)	50.5 (40.5)
$\|\chi^{(2)}_{122}(\omega)\|$ $Ag_2In_2GeSi_6$ ($Ag_2In_2SiSi_6$)	9.0 (8.0)	4.5 (4.0)	22.0 (12.0)	11.0 (6.0)
$\|\chi^{(2)}_{133}(\omega)\|$ $Ag_2In_2GeSi_6$ ($Ag_2In_2SiSi_6$)	7.0 (6.0)	3.5 (3.0)	34.0 (24.0)	17.0 (12.0)
$\|\chi^{(2)}_{221}(\omega)\|$ $Ag_2In_2GeSi_6$ ($Ag_2In_2SiSi_6$)	15.0 (13.0)	7.5 (6.5)	69.0 (56.0)	43.5 (28.0)
$\|\chi^{(2)}_{331}(\omega)\|$ $Ag_2In_2GeSi_6$ ($Ag_2In_2SiSi_6$)	21.0 (16.0)	10.5 (8.0)	85.0 (65.0)	42.5 (32.5)

glass plates on the routable table. The output signal was registered by photomultiplier, which spectrally cut the 532 nm green nanosecond fundamental pulses from a Nd:YAG laser operating at a wavelength of 1064 nm. As reference samples, crystals of BiB_3O_6 were used. The corresponding SHG angle dependences are given in Figure 5. One can see that, for the $Ag_2In_2GeS_6$ samples, the effective second order susceptibility is on average higher than that obtained for the $Ag_2In_2SiS_6$, and the corresponding values are equal to 1.25 pm/V and 0.97 pm/V. Their relative ratio is close to the theoretically calculated value. However, the absolute values are less, which may be caused partially by the energy gap underestimation, which is typical for the DFT approaches as well as due to the presence of intrinsic defects in the samples. Additionally, the phase matching conditions were not completely optimized. We should emphasize that the presented data are the so-called effective second order susceptibility becasue they are done for small samples, several hundred micrometers, while the direct comparison with calculated tensor components will require large bulk samples. It is necessary additionally to emphasize that effective second order susceptibilities present effective averaged different tensor components, which allow the comparison of relative values of susceptibilities while the absolute value comparison requires bigger samples.

We would like to mention here that in our previous works[27−29,33,35,36] we have calculated the linear and nonlinear

dx.doi.org/10.1021/jp311842v | J. Phys. Chem. B XXXX, XXX, XXX−XXX

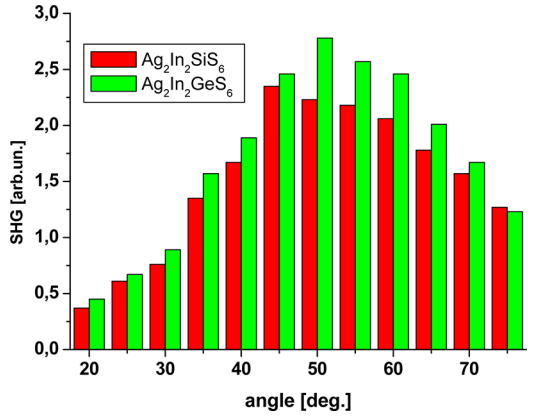

Figure 5. Angular dependence of SHG using the powder Kurtz Perry method. The samples with sizes within the 100−300 μm were put between the glass plates on the routable table. The output signal was registered by photomultiplier, which spectrally cut the 532 nm green nanosecond fundamental pulses from Nd:YAG laser operating at wavelength 1064 nm.

optical susceptibilities using FPLAPW method on several systems whose linear and nonlinear optical susceptibilities are known experimentally for the case of bulk crystals. We have found very good agreement with the experimental data. Thus, we believe that our calculations reported in this article would produce very accurate and reliable results in the case of the bulk samples.

The microscopic first order hyperpolarizability, β_{123}, vector component along the principal dipole moment directions for the dominant component $\chi^{(2)}_{111}(\omega)$ was obtained using the expression given in refs 33, 37, and 38:

$$\beta_{ijk} = \frac{\chi^{(2)}_{ijk}}{Nf^3}$$

where N is the number of molecules/cm^3 and f is the local field factor, the value of f is varying between 1.3 to 2.0. Using these information, we can estimate the value of first order hyperpolarizability tensor β_{ijk}. We have found that these values are equal to be 19.1× 10^{-30} (16.1× 10^{-30}) esu in the static limit for $Ag_2In_2GeS_6$ ($Ag_2In_2SiS_6$) and 57.1× 10^{-30} (43.9× 10^{-30}) esu at λ = 1064 nm (corresponding to 1.165 eV).

6. CONCLUSIONS

Using the all-electron full potential linearized augmented plane wave (FP-LAPW) method within the framework of the WIEN2K code, the linear and nonlinear optical susceptibilities dispersions were calculated for $Ag_2In_2SiS_6$ and $Ag_2In_2GeS_6$ crystals. The effect of replacing Si by Ge atom on the crystal structure and hence on the optical dispersions are explored. It is clear that the spectral features of $\varepsilon_2^{\text{average}}(\omega)$ for both crystals are similar except for a small increase in the amplitude of the left-hand hump of $\varepsilon_2^{\text{average}}(\omega)$ in $Ag_2In_2GeS_6$ and a small spectral shift of the main peak to lower energies. This difference could be attributed to the fact that replacing Si by Ge leads to migrate the S3, S4, and S6 atoms, which are directly connected to Si atom in $Ag_2In_2SiS_6$ to join In1 and In2 atoms in $Ag_2In_2GeS_6$ leaving the ends of In1 and In2 atoms in $Ag_2In_2GeS_6$ open. As a consequence, the band structures of both crystals show clear differences in the band splitting of the CB of $Ag_2In_2GeS_6$ with respect to $Ag_2In_2SiS_6$, and hence, the optical transitions are different. The second-order nonlinear optical susceptibilities, namely, SHG was calculated for five independent nonzero components. The influence of using different XC on the NLO susceptibilities, as well as the influence of replacing Si by Ge atom was investigated. The microscopic first order hyperpolarizability, β_{111}, vector component along the principal dipole moment directions for the dominant component $\chi^{(2)}_{111}(\omega)$ was obtained for the static limit and at λ = 1064 nm (corresponding to 1.165 eV). In summary, $Ag_2In_2GeS_6$ crystals show the highest values of the linear and nonlinear optical susceptibilities and the hyperpolarizability in comparison to $Ag_2In_2SiS_6$ crystal. The comparison of the experimentally measured SHG using Kurtz−Perry powder technique has shown a good agreement for the relative values of the second order susceptibilities; however, the absolute values have shown differences that are caused by the large number of defects and some underestimation of the energy gaps within the DFT approach.

AUTHOR INFORMATION

Corresponding Author

*Tel: +420 777 729 583. Fax: +420-386 361 219. E-mail: maalidph@yahoo.co.uk or reshak@frov.jcu.cz.

Notes

The authors declare no competing financial interest.

ACKNOWLEDGMENTS

This work was supported from the institutional research concept of the project CENAKVA (No. CZ.1.05/2.1.00/01.0024), the grant No. 152/2010/Z of the Grant Agency of the University of South Bohemia, and School of Material Engineering, Malaysia University of Perlis, Malaysia. S.A. would like to thank NPL for financial assistance. For I.V.K. this work is partially supported by Polish National Science Centre (project No. 2011/01/B/ST7/06194).

REFERENCES

(1) Lekse, J. W.; Moreau, M. A.; McNerny, K. L.; Yeon, J.; Halasyamani, P. S.; Aitken, J. A. Second-Harmonic Generation and Crystal Structure of the Diamond-Like Semiconductors Li_2CdGeS_4 and Li_2CdSnS_4. *Inorg. Chem.* **2009**, *48*, 7516−7518.

(2) Lekse, J. W.; Leverett, B. M.; Lake, C. H.; Aitken, J. A. Synthesis, Physicochemical Characterization and Crystallographic Twinning of Li_2ZnSnS_4. *J. Solid State Chem.* **2008**, *181*, 3217−3222.

(3) Matsushita, H.; Katsui, A. Materials Design for Cu-Based Quaternary Compounds Derived from Chalcopyrite-Rule. *J. Phys. Chem. Solids* **2005**, *66*, 1933−1936.

(4) Todorov, T. K.; Reuter, K. B.; Mitzi, D. B. High-Efficiency Solar Cell with Earth-Abundant Liquid-Processed Absorber. *Adv. Mater.* **2010**, *22*, E156−E159.

(5) Zhou, Z.; Wang, Y.; Xu, D.; Zhang, Y. Fabrication of Cu_2ZnSnS_4 Screen Printed Layers for Solar Cells. *Sol. Energy Mater. Sol. Cells* **2010**, *94*, 2042−2045.

(6) Davydyuk, G. E.; Myronchuk, G. L.; Kityk, I. V.; Danyl'chuk, S. P.; Bozhko, V. V.; Parasyuk, O. V. Ag_2CdSnS_4 Single Crystals As Promising Materials for Optoelectronic. *Opt. Mater.* **2011**, *33*, 1302−1306.

(7) Parasyuk, O. V.; Piskach, L. V.; Romanyuk, Y. E.; Olekseyuk, I. D.; Zaremba, V. I.; Pekhnyo, V. I. Phase Relations in the Quasi-Binary Cu_2GeS_3−ZnS and Quasi-Ternary Cu_2S−Zn(Cd)S−GeS2 Systems and Crystal Structure of Cu_2ZnGeS_4. *J. Alloys Compd.* **2005**, *397*, 85−94.

(8) Biswas, K.; Zhang, Q.; Chung, I.; Song, J.-H.; Androulakis, J.; Freeman, A. J.; Kanatzidis, M. G. Synthesis in Ionic Liquids: $[Bi_2Te_2Br](AlCl_4)$, a Direct Gap Semiconductor with a Cationic Framework. *J. Am. Chem. Soc.* **2010**, *132*, 14760−14762.

(9) Zhang, Q.; Chung, I.; Jang, J. I.; Ketterson, J. B.; Kanatzidis, M. G. Chalcogenide Chemistry in Ionic Liquids: Nonlinear Optical Wave-Mixing Properties of the Double-Cubane Compound $[Sb_7S_8Br_2]$-$(AlCl_4)_3$. *J. Am. Chem. Soc.* **2009**, *131*, 9896−9897.
(10) Zhang, Q.; Wu, T.; Bu, X.; Tran, T.; Feng, P. Ion Pair Charge-Transfer Salts Based on Metal Chalcogenide Clusters and Methyl Viologen Cations. *Chem. Mater.* **2008**, *20*, 4170−4172.
(11) Liu, Y..; Kanhere, P. D.; Wong, C. H.; Tian, Y.; Feng, Y.; Boey, F.; Wu, T.; Chen, H.; White, T. J.; Chen, Z.; Zhang, Q. Hydrazine-Hydrothermal Method to Synthesize Three-Dimensional Chalcogenide Framework for Photocatalytic Hydrogen Generation. *J. Solid-State Chem* **2010**, *183*, 2644−2649.
(12) Liu, Y.; Wei, F.; Yeo, S. N.; Lee, F. M.; Kloc, C.; Yan, Q.; Hng, H. H.; Ma, J.; Zhang, Q. Synthesis, Crystal Structure and Optical Properties of a Novel Three-Dimensional Quaternary Hg−In−S−Cl Chalcohalide: $Hg_7InS_6Cl_5$. *Inorg. Chem.* **2012**, *51*, 4414−4416.
(13) Fedorchuk, A. O.; Gorgut, G. P.; Parasyuk, O. V.; Lakshminarayana, G.; Kityk, I. V.; Piasecki, M. IR Operated Novel $Ag_{0.98}Cu_{0.02}GaGe_3Se_8$ Single Crystals. *J. Phys. Chem. Solids* **2011**, *72*, 1354−1357.
(14) Sachanyuk, V. P. Doctoral Thesis, L'viv National University, 2008.
(15) Chmiel, M.; Piasecki, M.; Myronchuk, G.; Lakshminarayana, G.; Reshak, A. H.; Parasyuk, O. G.; Kogut, Y.; Kityk, I. V. Optical and Photoconductivity Spectra of Novel $Ag_2In_2SiS_6$ and $Ag_2In_2GeS_6$ Chalcogenide Crystals. *Spectrochim. Acta, Part A* **2012**, *91*, 48−50.
(16) Reshak, A. H.; Khyzhun, O. Y.; Kityk, I. V.; Fedorchuk, A. O.; Kamarudin, H.; Auluck, S.; Parasyuk, O. V. Electronic Structure and the Influence of Replacing Ge by Si in the Chalcogenide Quaternary Sulfides $Ag_2In_2Ge(Si)S_6$ Single Crystals: Experiment XPS and XRD and Theory. *Sci. Adv. Mater.* **2013**, *5*, 1−12.
(17) Albert, I. D. L.; Marks, T. J.; Ratner, M. A. Rational Design of Molecules with Large Hyperpolarizabilities. Electric Field, Solvent Polarity, and Bond Length Alternation Effects on Merocyanine Dye Linear and Nonlinear Optical Properties. *J. Phys. Chem.* **1996**, *100*, 9714−9725.
(18) Blaha, P.; Schwarz, K.; Madsen, G. K. H.; Kvasnicka, D.; Luitz, J. *WIEN2K*, an Augmented Plane Wave + Local Orbitals Program for Calculating Crystal Properties; Karlheinz Schwarz Techn Universitat: Wien, Austria, 2001.
(19) Ceperley, D. M.; Ader, B. I. Ground State of the Electron Gas by a Stochastic Method. *Phys. Rev. Lett.* **1980**, *45*, 566−569. Parametrized in Perdew, J. P.; Zunger, A. One-Electron Theory of the Bulk Properties of Crystalline Ar, Kr, and Xe. *Phys. Rev. B* **1973**, *8*, 4822−4832.
(20) Perdew, J. P.; Burke, S.; Ernzerhof, M. Generalized Gradient Approximation Made Simple. *Phys. Rev. Lett.* **1996**, *77*, 3865−3868.
(21) Engel, E.; Vosko, S. H. Exact Exchange-Only Potentials and the Virial Relation as Microscopic Criteria for Generalized Gradient Approximations. *Phys. Rev. B* **1993**, *47*, 13164−13174.
(22) Tran, F.; Blaha, P. Accurate Band Gaps of Semiconductors and Insulators with a Semilocal Exchange-Correlation Potential. *Phys. Rev. Lett.* **2009**, *102*, 226401−226404.
(23) Bader, R. F. W. Atoms in Molecules. In *A Quantum Theory*; Oxford University Press: Oxford, U.K., 1990.
(24) Reshak, A. H. Electronic, Linear and Non-Linear Optical Properties of Transition Metal Dichalcogenides. Ph.D. Thesis, Indian Institute of Technology, 2005.
(25) Tributsch, H. *Z. Naturforsch.* **1977**, *A 32A*, 972.
(26) Penn, D. R. Wave-Number-Dependent Dielectric Function of Semiconductors. *Phys. Rev.* **1962**, *28*, 2093−2097.
(27) Reshak, A. H.; Kityk, I. V.; Auluck, S. Investigation of the Linear and Nonlinear Optical Susceptibilities of $KTiOPO_4$ Single Crystals: Theory and Experiment. *J. Phys. Chem. B* **2010**, *114*, 16705−16712.
(28) Reshak, A. H.; Auluck, S.; Kityk, I. V. Linear and Nonlinear Optical Susceptibilities for a Novel Borate Oxide $BaBiBO_4$: Theory and Experiment. *J. Solid State Chem.* **2008**, *181*, 789−795.
(29) Reshak, A. H.; Auluck, S.; Kityk, I. V. Optical Susceptibilities of $Na_3La_9O_3(BO_3)_8$, Ternary Oxyborate Nonlinear Single Crystal: Theory and Experiment. *J. Phys.: Condens. Matter* **2008**, *20*, 145209−145215.
(30) Reshak, A. H.; Auluck, S.; Kityk, I. V. Experimental and Theoretical Investigations of the First and Second Order Optical Susceptibilities of BiB_3O_6 Single Crystal. *Appl. Phys. A: Mater. Sci. Process.* **2008**, *91*, 451−457.
(31) Reshak, A. H.; Auluck, S. Electronic Structure, Linear, Nonlinear Optical Susceptibilities and Birefringence of $CuInX_2$ (X = S, Se, Te) Chalcopyrite-Structure Compounds. *PMC Phys. B* **2008**, 1:12.
(32) Reshak, A. H.; Auluck, S.; Kityk, I. V. Several Features of Nonlinear Optical Susceptibilities of $LiGaX_2$ (*X* = S, Se) Ternary Compounds. *J. Alloys Compd.* **2009**, *473*, 20−24.
(33) Reshak, A. H.; Auluck, S.; Stys, D.; Kityk, I. V.; Kamarudin, H.; Berdowski, J.; Tylczynski, Z. Dispersion of Linear and Non-Linear Optical Susceptibilities for Amino Acid 2-Aminopropanoic $CH_3CH(NH_2)COOH$ Single Crystals: Experimental and Theoretical Investigations. *J. Mater. Chem.* **2011**, *21*, 17219−17228.
(34) Kurtz, S. K.; Perry, T. T. A Powder Technique for the Evaluation of Nonlinear Optical Materials. *J. Appl. Phys.* **1968**, *39*, 3798−3813.
(35) Reshak, A. H. Theoretical Investigation of the Electronic Properties, and First and Second Harmonic Generation for Cadmium Chalcogenide. *J. Chem. Phys.* **2006**, *124*, 104707−104712.
(36) Reshak, A. H. First-Principle Calculations of the Linear and Nonlinear Optical Response for GaX (X = As, Sb, P). *Eur. Phys. J. B* **2005**, *47*, 503−508.
(37) Boyd. R. Y. *Principles of Nonlinear Optics*; Academic Press: New York, 1982; p 420.
(38) Boyd, R. W. *Nonlinear Optics*, 3rd ed.; Academic Press: New York, 2008.